Lab on a Chip

PAPER

View Article Online
View Journal

Cite this: DOI: 10.1039/c6lc01455k

The microfluidic nebulator: production of sub-micrometer sized airborne drops†

Esther Amstad,*[ab] Frans Spaepen,[a] Michael P. Brenner[a] and David A. Weitz[ac]

Many powders employed in the food and pharmaceutical industries are produced through spray drying because it is a cost efficient process that offers control over the particle size. However, most commercially available spray-driers cannot produce drops with diameters below 1 μm, limiting the size of spray-dried particles to values above 300 nm. We recently developed a microfluidic spray-drier that can form much smaller drops than commercially available spray-driers. This is achieved through a two-step process: first, the microfluidic spray-drier operates in the dripping regime to form 100 μm diameter primary drops in air and, second, subjects them to high shear stresses due to supersonic flow of air to break them into many much smaller secondary drops. In this paper, we describe the two essential steps required to form sub-μm diameter airborne drops inside microfluidic channels. We investigate the influence of the device geometry on the ability to operate the microfluidic spray-drier in the dripping regime. Moreover, we describe how these primary drops are nebulized into many secondary drops that are much smaller than the smallest dimension of the spray-drier channels.

Received 28th November 2016,
Accepted 10th March 2017

DOI: 10.1039/c6lc01455k

rsc.li/loc

Introduction

Spray-driers are often employed to process solutions and dispersions into dry powders by breaking solute-containing fluids into airborne drops that are subsequently dried in a stream of hot air.[1,2] This process is cost effective and offers good control over the drop size, which enables tuning the size of spray dried particles. Hence, it is commonly employed for the formulation of active ingredients, for example in the food,[3] cosmetic,[4] and pharmaceutical industries.[1] Many of these applications require good control over the dissolution kinetics of the resultant spray-dried particles, which increases with their surface-to-volume ratio, and hence with decreasing particle size.[5,6] Production of small particles requires the formation of small drops. The size of drops produced in typical commercially available spray-driers is of the order of the nozzle diameter,[2] limiting their minimum size to that of nozzles that can still be reliably fabricated and operated. Typical commercially available instruments produce drops with diameters ranging from 10 μm to 100 μm,[7] resulting in particles with diameters between 5 μm and several 10s of μm. Commercially available instruments designed to produce small drops can generate drops with diameters down to 3 μm, resulting in particle-diameters between 350 nm and 1 μm.[8] By contrast, microfluidic spray-driers can produce drops with diameters much smaller than the smallest dimension of their nozzles.[9,10] For example, the microfluidic nebulator produces drops with diameters as small as 300 nm.[10] The production of such small drops is made possible by a new nozzle design that allows formation of airborne aqueous primary drops in the dripping regime and subsequently subjects them to very high shear stresses to break them into secondary drops. This is in stark contrast to previously reported microfluidic devices that form airborne aqueous drops in a single step and outside the microfluidic channel; these devices operate exclusively in the jetting regime and do not form the secondary drops.[9] The dripping-to-jetting transition has been shown to strongly depend on the design and operation conditions of microfluidic devices used to produce emulsion drops.[11–14] However, this transition has never been explored for microfluidic spray-driers despite its importance for formation of drops in air; moreover, the influence of device geometry on the nebulization or on-chip formation of such small airborne secondary drops has also never been explored.

In this paper, we describe how airborne aqueous sub-μm diameter drops can be formed inside a microfluidic spray-drier. We demonstrate the influence of the nozzle geometry on the dripping-to-jetting transition in microfluidic spray-driers. Moreover, we investigate how these primary drops are accelerated and subjected to supersonic air flow, which

[a] School of Engineering and Applied Sciences, Harvard University, Massachusetts 02138, USA
[b] Institute of Materials, Ecole Polytechnique Fédérale de Lausanne (EPFL), Switzerland. E-mail: esther.amstad@epfl.ch
[c] Department of Physics, Harvard University, Massachusetts 02138, USA

† Electronic supplementary information (ESI) available. See DOI: 10.1039/c6lc01455k

nebulizes them and forms many much smaller secondary drops that produce nanoparticles with sizes down to 12 nm.

Experimental

Microfluidic spray-drier

The microfluidic spray-drier is made of poly(dimethyl siloxane) (PDMS) using soft lithography.[15] The device contains two inlets for liquids and two to six inlets for air. The liquid inlets and all the air inlets except of the last one are 100 μm tall. The last air inlet is 300 μm tall to form a three dimensional junction. To make the channel walls non-wetting, we treat them with dodecane containing 3 wt% trichlorododecylsilane.

Production of $CaCO_3$ nanoparticles

$CaCO_3$ nanoparticles are produced through a precipitation reaction that is initiated inside the microfluidic spray-drier immediately before drops form. We inject an aqueous solution containing 5 mM $CaCl_2$ at 0.5 mL h^{-1} into the first liquid inlet using syringe pumps. Simultaneously, we inject an aqueous solution containing 5 mM Na_2CO_3 at 0.5 mL h^{-1} into the second liquid inlet. We keep the pressure at all the air inlets constant at 0.28 MPa. The spray-dried particles are collected 25 cm apart from the device outlet on a one-side polished Si-wafer.

Quantification of the size of secondary drops

We calculate the size of secondary drops from the measured size of spray-dried $CaCO_3$ nanoparticles. To convert the nanoparticle size into the size of secondary drops when they form, we assume that each secondary drop produces exactly one $CaCO_3$ particle. We assume that the solvent evaporation in primary drops is negligible before the secondary drops are formed, because the air velocity in the initial parts of the microfluidic spray-drier is low and the residence time of primary drops in the microfluidic spray-drier is very short. Hence, we approximate the solute concentration when secondary drops form to be equal to that of the mixture of the injected solutions. To convert the volume of a particle into its mass, we assume the density of the $CaCO_3$/NaCl mixture to be 2.34 g cm^{-3}.

Results and discussion

We produce aqueous drops in a stream of air using a microfluidic spray-drier, a nebulator, made from poly(dimethyl siloxane) (PDMS) using soft lithography.[15] The nebulator contains inlets for two liquids and multiple pairs of inlets for air, as shown schematically in Fig. 1. The last junction is three dimensional (3D) with a 100 μm tall main channel opening into a 300 μm tall channel;[16] this geometry minimizes the risk that drops contact the channel walls in the final part of the nebulator. Drops exit the device through a nozzle made by cutting the main channel with a razor blade.[9,10]

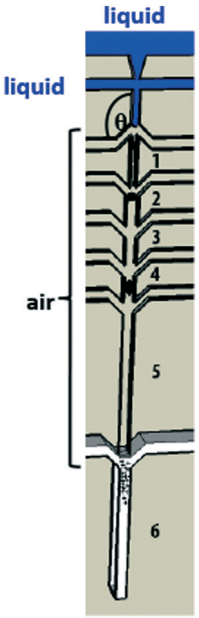

Fig. 1 Schematic illustration of the optimized nebulator. The main channel is divided into channel sections 1–6. The first pair of air inlets intersects the main channel at θ = 135°, the subsequent air inlets intersect the main channel at 45°.

To produce drops at the first air–liquid junction, the channel walls must be strongly non-wetting. To produce aqueous drops in air, we treat the channel walls with a solution of dodecane containing 50 wt% dodecyltriethoxysilane. We regulate the airflow with the pressure applied to the inlets, keeping the pressure at all the entrances the same. We inject water into one liquid inlet using pumps and block the second liquid inlet, which is included in the design to have the flexibility to mix two fluids prior to the spray-dry process. The second liquid inlet is blocked using poly(ethylene) tubing that is sealed on one side.

The nebulator uses air as a continuous phase; its dynamic viscosity is approximately three orders of magnitude lower than that of water or oils typically used in microfluidic devices. This much lower viscosity results in a distinctly different fluid dynamic behavior. To visualize drop formation in the nebulator, we use a high-speed camera operated at 38 000 frames per second. Nebulators containing only one or two pairs of air inlets pull the liquid into a thin jet that uncontrollably breaks at the nozzle, resulting in drops with a broad size distribution, as shown in the top optical micrograph in Fig. 2a. To improve the control over the drop size, we must form them on chip.

A possibility to form drops inside the nebulator is its operation in the dripping regime; this requires an absolute instability in the fluid.[17] This instability develops if the component of the air velocity directed along the main channel, $\vec{v}$, is very low and thus does not pull the liquid into a jet. We decrease the velocity of the air at the first air–liquid junction by injecting it through multiple inlets; this reduces the pressure gradients between adjacent junctions. To quantify the air

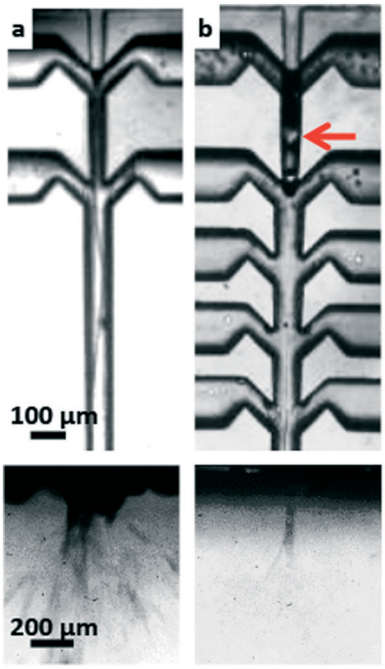

Fig. 2 Optical micrographs of the main channel (top) and nozzle (bottom) of a nebulator with θ = 45° containing (a) two and (b) five pairs of 2D air inlets. Both nebulators have one additional pair of inlets that form the 3D junction. (a) The liquid is pulled into a thin jet that retains its integrity until it reaches the nozzle. (b) The liquid forms long aqueous plugs. The leading edge of a forming plug is indicated with the red arrow.

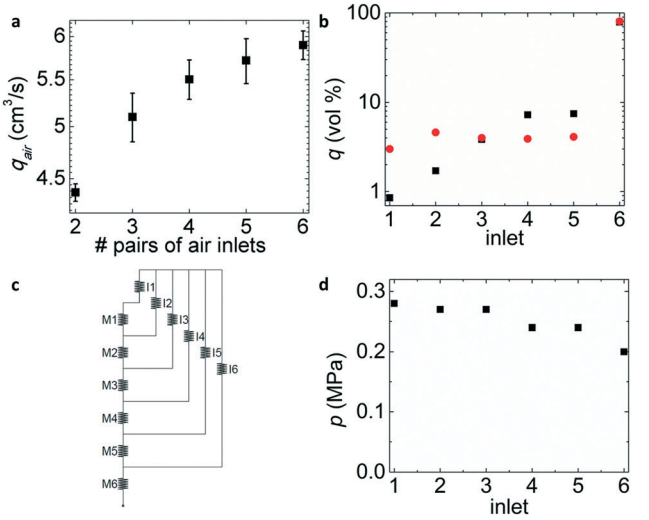

Fig. 3 (a) Influence of the number of inlets supplied with air on its flux at the last two-dimensional junction. (b) Volume fraction of air that flows through each pair of inlets, determined by subtracting fluxes from adjacent air inlets without taking into account possible couplings (■) and calculated using the Kirchhoff's law (●). (c) Schematic illustration of an electric circuit analogue of the nebulator used to calculate the flux with the Kirchhoff's law. I1–I6 denote the resistances of the air inlets, M1–M6 those of the main channel sections. (d) Pressure at the different junctions measured by quantifying the pressure-dependent expansion of the channels using confocal microscopy.

flux, q, in the different parts of the main channel, we measure the flux at the outlet of devices containing different numbers of air inlets. We connect an empty, gas-tight syringe to the outlet and measure the time required to fill it with air. The flux at the outlet increases with the number of inlets supplied with air, as shown in Fig. 3a. We attribute the increase in q, obtained by supplying one additional pair of inlets with air, to the air flux through this added inlet pair. Accounting for the pressure-dependent density of the air, we determine the flux in each channel section; it is close to zero in the initial parts of the main channel and strongly increases towards the outlet, as shown by the black squares in Fig. 3b. Less than 3% of the volume of the air flows through the first pair of air inlets, as shown by the red circles in Fig. 3b. The vast majority, 80 vol%, flows through the last pair of inlets. Thus, we minimize the air flux in the initial parts of the main channel by injecting it through multiple inlets.

To facilitate optimization of the flow profile in the microfluidic device, it would be desirable to estimate this flow profile using simple equations. The flow in standard microfluidic devices can be computed using the Poiseuille law. To test if we can use this law to estimate the flow profile in the microfluidic spray-drier, despite of the high air velocity, we calculate the air flux, $q = \frac{\Delta p w^3 h\left(1-0.63\frac{h}{w}\right)}{12\mu_a L}$, in each side channel using an electric circuit analogue, as shown schematically in Fig. 3c, and Kirchhoff's law; here, Δp is the pressure drop, w the channel width, h its height, μ_a the dynamic viscosity of the air, and L is the length of the respective channel part.[18] We measure the pressure drop across each inlet channel by quantifying the small, but still measurable, pressure-dependent expansion of the PDMS channels using confocal microscopy, and convert it into a pressure profile using a calibration curve, shown in Fig. S1 and the channel dimensions shown in Table S1.† The pressure gradient is very small in the initial parts of the main channel and increases towards the nozzle, as shown in Fig. 3d. Using the measured values for Δp we calculate q in the different channel sections, ignoring any deformation of the channels due to the pressure as this changes the resistance by at most a few percent. In the first four channel sections, the flux profile calculated by subtraction of fluxes from adjacent channels shows some deviations from the one calculated using Kirchhoff's law, as shown in Fig. 3b. These results indicate that the air flow in the nebulator shows some deviations from the Poiseuille flow. Nevertheless, these crude and simple calculations provide a fair estimate of the flow profile.

For the nebulator to produce drops controllably, it must operate in the dripping regime. This requires a very low air velocity at the first air–liquid junction. However, even if nebulators possess as many as six pairs of air inlets, the velocity component along the main channel at the first air–liquid junction is still too high for the device to operate in the dripping regime. The flowing air breaks the water into long,

irregular plugs at the first air–liquid junction, as shown in the top optical micrograph of Fig. 2b. These plugs wet the channel walls downstream and break into smaller drops at the device outlet, as shown in the optical micrograph of the outlet at the bottom of Fig. 2b. The size of these drops is significantly smaller than if produced from jets, but their distribution is still broad.

To operate the device in the dripping regime, we must decrease $\vec{v}$ in the initial parts of the main channel even more. Incorporating additional air inlets is impractical. Instead, we make a simple, but very effective modification to the first air–liquid junction: we invert the direction of the first pair of air inlets. These inlets intersect the main channel at an angle θ = 135°, as shown schematically in Fig. 1. This modification forces the air to reverse its flow direction when entering the main channel, and thus must slow the velocity component parallel to the main channel to zero, creating a stagnation point. Indeed, nebulators with θ = 135° and at least three pairs of air inlets operate in a stable dripping regime, as shown in Fig. 4a–d and Movie S1.† The drop generation frequency increases nearly linearly with water flow rates increasing from 0.25 ml h^{-1} to 3 ml h^{-1}, as shown in Fig. 4e. The increase in drop generation frequency overcompensates the increase in flow rate such that the drop size decreases, as shown in Fig. 4f. However, once the flow rate exceeds 3 ml h^{-1}, a transition from the dripping into the jetting regime occurs, resulting in a broadening of the drop size distribution. This transition sets an upper limit to the throughput of an individual nebulator.

An important feature of the nebulator is its ability to produce sub-μm sized airborne drops. This can be achieved by subjecting them to high shear stresses, which requires the air velocity to be high. To enable this break-up, we accelerate the air from stagnation to very high velocities by successively injecting air into the main channel through additional inlets.[10] The fast-flowing air deforms the drops at each junction, as exemplified in the time-lapse optical micrographs in Fig. 4b–d. This deformation strongly increases the shear stress, $\tau = \mu_a \frac{dv}{l}$, because it decreases the distance between the drop surface and the channel wall, l; here dv is the difference in velocity of the air and the drops. In addition, this deformation locally increases the air velocity and hence dv, because the flux remains constant but the cross section of the channel, through which the air can flow, is locally much smaller. The high air flux and strong drop deformation result in a high local air velocity, which causes the primary drop to break into many much smaller secondary drops.

The nebulator produces airborne drops that are much smaller than the smallest dimension of the main channel. Hence, the minimum size of drops the nebulator can produce is not limited by the size of the orifice, in distinct contrast to commercial spray driers. Instead, we expect this size to depend on the shear stress, which strongly increases towards the exit. To estimate the evolution of the shear stress in the nebulator, we monitor primary drops as they fly towards the exit. The primary drop velocity is very low in channel sections 1 and 2 and significantly increases in channel sections 3 and 4, as shown in Fig. 5a. While primary drops are accelerated, their velocity distribution is broadened, as indicated by the larger error bars in Fig. 5a. However, because the air flows at least 10 times faster than primary drops do, the difference in the velocities remains very large, even though the drop velocity varies somewhat. As a result, each primary drop is exposed to shear stresses that are large and of the same order of magnitude. We are unable to visualize drops in channel section 5, suggesting that the break-up of primary drops occurs at this location.

To investigate the conditions under which primary drops break up, we quantify the local velocity of the air as it enters channel section 5. We measure the air flux, q, in this channel section to be 5.7 cm^3 s^{-1}. We convert this flux into a velocity using $v = \frac{q}{A}\frac{\rho_o}{\rho_c}$; here A is the channel cross-section in section

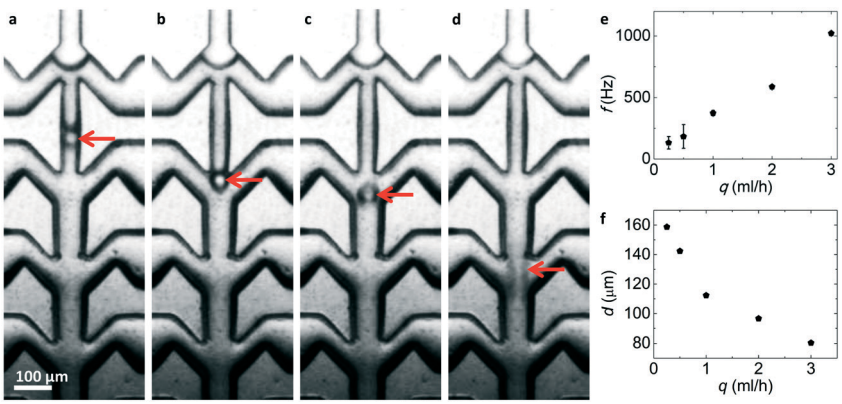

Fig. 4 (a–d) Time-lapse optical micrographs of a nebulator with θ = 135° and five pairs of 2D air inlets, one pair of 3D inlets; the fifth and sixth pairs of air inlets are outside the field of view. Images are taken (a) 120 μs, (b) 180 μs, (c) 240 μs, and (d) 300 μs after the drop pinched off. The red arrows indicate the location of the drop, which is in (d) is blurred because of its strong acceleration, resulting in a high speed. (e) Drop generation frequency and (f) drop diameter as a function of the water injection rate. The pressure applied to all the air inlets is 0.28 MPa.

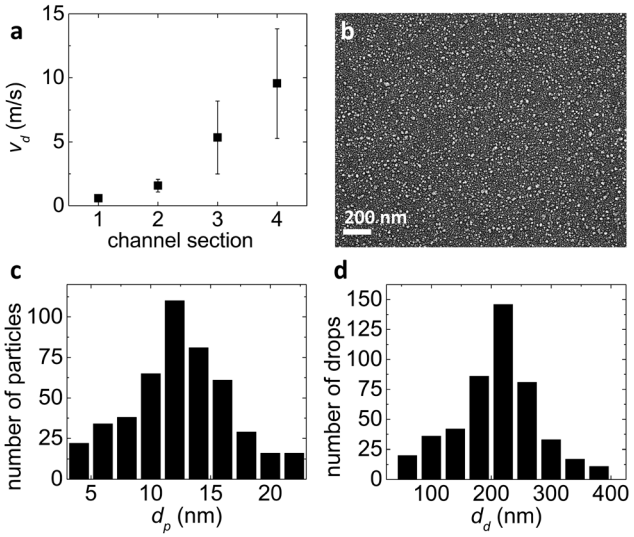

Fig. 5 (a) Velocity of primary drops as a function of the channel section. The pressure applied to all six air inlets is 0.28 MPa. (b) SEM image of spray-dried $CaCO_3$ nanoparticles (c) with their size distribution. (d) The size distribution of drops calculated from the measured size distribution of $CaCO_3$ particles.

5, which is 8000 μm^2, ρ_o the density of air at the outlet, which we take as 1.225 kg m^{-3} and ρ_c the density in the channel section. To determine ρ_c, we use the Redlich–Kwong equation of state and the measured pressure in this channel section, shown in Fig. 3d. We obtain ρ_c = 2.1 kg m^{-3}, which results in a velocity of 420 m s^{-1}; this is higher than the speed of sound in air at 1 bar, which is 340 m s^{-1}. The local velocity in the vicinity of the drops is even higher, because they effectively reduce the cross-section of the main channel through which the air flows at a constant flux. To estimate this local velocity, we divide the flux by the effective cross-section of the channel in the presence of a deformed drop by measuring l, using optical micrographs, and multiplying this value with the channel height. If secondary drops form under subsonic conditions, their diameter would be determined by the balance of the shear stress and the Laplace pressure, $\mu \frac{dv}{l} = \frac{2\gamma}{r}$; here γ is the surface tension and r the radius of the secondary drop. We assume that this is also the case for drops formed under supersonic conditions and we therefore calculate the drop diameter to be 500 nm.

In these calculations we assume that the drop diameter is determined by balancing the shear stress and the Laplace pressure. To test this assumption experimentally, we spray-dry $CaCO_3$ nanoparticles. These particles have an average diameter as small as 12 nm, as shown in the scanning electron microscopy (SEM) image in Fig. 5b and display a relatively narrow size distribution, as determined by image analysis and summarized in Fig. 5c and Table S2.† Assuming that the solute concentration when secondary drops form is equal to that of the mixture of the injected solutions, the average initial diameter of secondary drops must be 200 nm and their coefficient of variation, defined as the standard deviation of their diameter divided by its mean, is 38%, as summarized in Fig. 5d and Table S3.† These experimentally measured sizes are consistent with the calculated values.

The yield of spray-dried nanoparticles increases with decreasing distance between the nozzle outlet and the collection tube, as fewer particles get lost during the drying process. To minimize this distance, we must maximize the evaporation rate. The nebulator dries water very quickly: the fast-flowing air makes the boundary layer that surrounds the secondary drop very thin, thereby facilitating the transport of evaporating water molecules away from the drop surface. To estimate the diffusion time of water molecules across the boundary layer, we calculate the boundary layer thickness, $\delta = \frac{r}{\mathrm{Pe}^{\frac{1}{3}}}$; here r is the radius of the secondary drop and Pe the Péclet number, which we compute using the speed of the air in the microfluidic channel. The boundary layer is only 15 nm; this is thinner than the mean free path of a water molecule in air at 1 bar. Hence, the diffusion of molecules across the boundary layer is faster than their removal from the surface. As a result, the evaporation rate is limited by the rate at which molecules leave the surface, which, by detailed balance, equals the rate at which gas molecules, in equilibrium, impinge the area of the drop surface, A. Kinetic theory gives $z = \frac{N}{A\Delta t} = \frac{p_{vap}}{\sqrt{2\pi m_m k_B T}}$; here N is the number of molecules that leave the drop surface area in a given amount of time Δt, p_{vap} is the equilibrium vapor pressure of the solvent, and m_m the mass of a single molecule. This very fast evaporation allows collection of fully dried nanoparticles only 15 cm away from the nozzle; if collected at shorter distances the drops are visually determined to still be wet.

Conclusion

The nebulator produces aqueous, airborne drops with diameters much smaller than any of its channel dimensions. This is enabled through a two-step process: primary drops with diameters similar to the channel width are formed by operating the microfluidic spray-drier in the dripping regime; this operation requires the air velocity at the first air–liquid junction to be close to stagnation. To facilitate operation of the microfluidic spray-drier in the dripping regime, we push the dripping-to-jetting transition to higher injection air pressures by making a simple but effective change to the junction geometry: we inject the air from the opposite direction to the fluid flow. To break these primary drops into much smaller secondary drops, they must be subjected to high shear stresses, which requires the air velocity to be very high. The microfluidic spray-drier accelerates the air from close to stagnation to supersonic speeds. This fast flowing air exerts such

a high shear stress on primary drops that they break into many much smaller secondary drops. To calculate the size of secondary drops we assume that the drop size is determined by the balance of the shear stress and Laplace pressure, which is true if the air velocity is low. However, in our case, the air velocity is 20% higher than the speed of sound at 1 bar; it is as high as 420 m s^{-1}. Even though these air velocities are extremely high, our calculated drop sizes are consistent with the experimentally determined values. The supersonic speed of the air reached towards the exit of the device adds an additional advantage: it rapidly dries drops. This fast solvent evaporation makes the use of hot air, typically employed in spray-driers, unnecessary, such that even thermo-labile substances can be processed with this device. The mechanism of drop formation is qualitatively different from that employed in other spray driers. By refining the two-step drop formation process even further improvements of the microfluidic spray-dry nozzle should be feasible.

Acknowledgements

This work was financially supported by the NSF (DMR-1310266) and the Harvard MRSEC (DMR-1420570). MPB was supported by NSF-DMS1411694 and is an investigator of the Simons Foundation. Part of this work was performed at the Center for Nanoscale Systems (CNS), a member of the National Nanotechnology Infrastructure Network (NNIN), which is supported by the National Science Foundation under NSF award no. ECS-0335765. CNS is part of Harvard University.

References

1 A. Paudel, Z. A. Worku, J. Meeus, S. Guns and G. Van den Mooter, *Int. J. Pharm.*, 2013, **453**, 253–284.
2 K. Cal and K. Sollohub, *J. Pharm. Sci.*, 2010, **99**, 575–586.
3 R. Murugesan and V. Orsat, *Food Bioprocess Technol.*, 2012, **5**, 3–14.
4 K. Okuyama, M. Abdullah, I. W. Lenggoro and F. Iskandar, *Adv. Powder Technol.*, 2006, **17**, 587–611.
5 Y. Kawabata, K. Wada, M. Nakatani, S. Yamada and S. Onoue, *Int. J. Pharm.*, 2011, **420**, 1–10.
6 J. Sun, F. Wang, Y. Sui, Z. She, W. Zhai, C. Wang and Y. Deng, *Int. J. Nanomed.*, 2012, **7**, 5733–5744.
7 S.-T. Corp, http://www.sono-tek.com/drop-size-and-distribution/).
8 C. Arpagaus, *Drying Technol.*, 2012, **30**, 1113–1121.
9 J. Thiele, M. Windbergs, A. R. Abate, M. Trebbin, H. C. Shum, S. Forster and D. A. Weitz, *Lab Chip*, 2011, **11**, 2362–2368.
10 E. Amstad, M. Gopinadhan, C. Holtze, C. O. Osuji, M. P. Brenner, F. Spaepen and D. A. Weitz, *Science*, 2015, **349**, 956–960.
11 A. S. Utada, A. Fernandez-Nieves, H. A. Stone and D. A. Weitz, *Phys. Rev. Lett.*, 2007, **99**, 094502.
12 C. Clanet and J. C. Lasheras, *J. Fluid Mech.*, 1999, **383**, 307–326.
13 C. Cramer, P. Fischer and E. J. Windhab, *Chem. Eng. Sci.*, 2004, **59**, 3045–3058.
14 B. Ambravaneswaran, H. J. Subramani, S. D. Phillips and O. A. Basaran, *Phys. Rev. Lett.*, 2004, **93**, 034501.
15 Y. N. Xia and G. M. Whitesides, *Angew. Chem., Int. Ed.*, 1998, **37**, 551–575.
16 A. Rotem, A. R. Abate, A. S. Utada, V. Van Steijn and D. A. Weitz, *Lab Chip*, 2012, 4263–4268.
17 S. P. Lin and Z. W. Lian, *Phys. Fluids A*, 1989, **1**, 490–493.
18 M. Tanyeri, M. Ranka, N. Sittipolkul and C. M. Schroeder, *Lab Chip*, 2011, **11**, 1786–1794.

